REPORT SSD-TR-90-45

AEROSPACE REPORT NO.
TR-0090(5925-01)-1

The Role of Acceptor Density on the High Channel Carrier Density I-V Characteristics of AlGaAs/GaAs MODFETs

Prepared by

R. J. KRANTZ and W. L. BLOSS
Electronics Research Laboratory
Laboratory Operations

19 October 1990

Prepared for

SPACE SYSTEMS DIVISION
AIR FORCE SYSTEMS COMMAND
Los Angeles Air Force Base
P.O. Box 92960
Los Angeles, CA 90009-2960

Development Group

THE AEROSPACE CORPORATION
El Segundo, California

This report was submitted by The Aerospace Corporation, El Segundo, CA 90245, under Contract No. F04701-88-C-0089 with the Space Systems Division, P.O. Box 92960, Los Angeles, CA 90009-2960. It was reviewed and approved for The Aerospace Corporation by M. J. Daugherty, Director, Electronics Research Laboratory. Captain Janet Modl was the Air Force project officer for the Mission-Oriented Investigation and Experimentation (MOIE) program.

This report has been reviewed by the Public Affairs Office (PAS) and is releasable to the National Technical Information Service (NTIS). At NTIS, it will be available to the general public, including foreign nationals.

This technical report has been reviewed and is approved for publication. Publication of this report does not constitute Air Force approval of the report's findings or conclusions. It is published only for the exchange and stimulation of ideas.

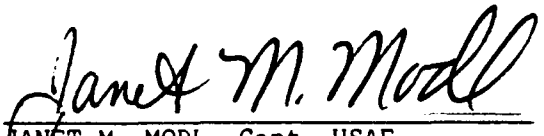

JANET M. MODL, Capt, USAF
MOIE Project Officer
STC/SWL

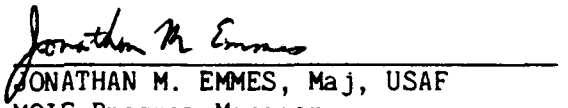

JONATHAN M. EMMES, Maj, USAF
MOIE Program Manager
AFSTC/WCO OL-AB

UNCLASSIFIED

SECURITY CLASSIFICATION OF THIS PAGE

REPORT DOCUMENTATION PAGE

1a. REPORT SECURITY CLASSIFICATION Unclassified	1b. RESTRICTIVE MARKINGS
2a. SECURITY CLASSIFICATION AUTHORITY	3. DISTRIBUTION/AVAILABILITY OF REPORT Approved for public release; distribution is unlimited
2b. DECLASSIFICATION/DOWNGRADING SCHEDULE	
4. PERFORMING ORGANIZATION REPORT NUMBER(S) TR-0090(5925-01)-1	5. MONITORING ORGANIZATION REPORT NUMBER(S) SSD-TR-90-45
6a. NAME OF PERFORMING ORGANIZATION The Aerospace Corporation Laboratory Operations 6b. OFFICE SYMBOL *(If applicable)*	7a. NAME OF MONITORING ORGANIZATION Space Systems Division
6c. ADDRESS *(City, State, and ZIP Code)* El Segundo, CA 90245	7b. ADDRESS *(City, State, and ZIP Code)* Los Angeles Air Force Base Los Angeles, CA 90009-2960
8a. NAME OF FUNDING/SPONSORING ORGANIZATION 8b. OFFICE SYMBOL *(If applicable)*	9. PROCUREMENT INSTRUMENT IDENTIFICATION NUMBER F04701-88-C-0089
8c. ADDRESS *(City, State, and ZIP Code)*	10. SOURCE OF FUNDING NUMBERS PROGRAM ELEMENT NO. / PROJECT NO / TASK NO. / WORK UNIT ACCESSION NO.

11. TITLE *(Include Security Classification)*
The Role of Acceptor Density on the High Channel Carrier Density I-V Characteristics of AlGaAs/GaAs MODFETs

12. PERSONAL AUTHOR(S)
Krantz, Richard J. and Bloss, Walter L.

13a. TYPE OF REPORT	13b. TIME COVERED	14. DATE OF REPORT *(Year, Month, Day)*	15. PAGE COUNT
	FROM _____ TO _____	1990 October 19	19

16. SUPPLEMENTARY NOTATION

17. COSATI CODES			18. SUBJECT TERMS *(Continue on reverse if necessary and identify by block number)*
FIELD	GROUP	SUB-GROUP	MODFETs Threshold Voltage High Density Operation

19. ABSTRACT *(Continue on reverse if necessary and identify by block number)*

A triangular-well, one-subband depletion layer model has been developed for the high density region of a modulation doped field-effect transistor (MODFET). High density operation is defined as operation when the channel carrier density, in the entire channel, is equal to or greater than $m_1 kT/\pi h^2$. This high density model has been used to describe the effects of the depletion layer charge on the I-V characteristics. An approximation for the experimentally determined threshold voltage is derived. For small acceptor densities, $\sim 10^{13}$ cm^{-3}, it is shown that the experimentally determined threshold voltage may differ from the strong inversion threshold voltage by ~0.25 V. We show that this discrepancy is due to the effect of the depletion layer charge in the high density region. Also, the depletion layer charge is shown to account for the discrepancy in the device capacitance and the AlGaAs layer capacitance. The effective layer thickness Δd is shown to decrease from ~90 Å at an acceptor density of 10^{13} cm^{-3} to 75 Å at 10^{17} cm^{-3}.

20. DISTRIBUTION/AVAILABILITY OF ABSTRACT	21. ABSTRACT SECURITY CLASSIFICATION
☒ UNCLASSIFIED/UNLIMITED ☐ SAME AS RPT ☐ DTIC USERS	Unclassified
22a. NAME OF RESPONSIBLE INDIVIDUAL	22b. TELEPHONE *(Include Area Code)* / 22c. OFFICE SYMBOL

DD FORM 1473, 84 MAR 83 APR edition may be used until exhausted. All other editions are obsolete

SECURITY CLASSIFICATION OF THIS PAGE

UNCLASSIFIED

CONTENTS

FIGURES

I. INTRODUCTION

The dependence of the threshold voltage, subthreshold I-V characteristics, and radiation response of n-channel AlGaAs/GaAs MODEFTs (modulation doped field-effect transistors) on acceptor doping density has been described previously (Refs. 1-4). These analyses have now been extended to describe the dependence of MODFET high channel carrier density I-V characteristics on acceptor doping density. The effect of acceptor doping density on the experimental threshold voltage and device capacitance is explicitly addressed.

The band structure of a typical AlGaAs(n)/GaAs heterojunction with Schottky barrier, ϕ_m, at the gate, and a spacer layer at the interface under bias V_g, is shown in Fig. 1. In the depletion layer approximation, the donors and acceptors are assumed to be completely ionized in the doped AlGaAs layer d, the spacer layer a, and in the depletion layer W. The doping densities N_D and N_A are assumed constant. The quasi-two-dimensional electron eigenstates at the interface are solved for using a triangular potential well, and only the lowest subband is included in the calculation. A delta-function channel charge distribution at the average channel width is assumed. Band bending from the interface at (d + a) to the edge of the depletion region (W + d + a) is the difference of the position of the conduction band relative to the Fermi level in the GaAs far from the interface ($E_g/2 + \phi_{bulk}$), and the Fermi level E_f relative to the bottom of the two-dimensional channel.

Under the restrictions imposed by these assumptions, Poisson's equation may be integrated across the structure to obtain the applied gate voltage as a function of device geometry, doping densities, and channel charge n_s:

$$V_g = \phi_m - \Delta E_c + E_f + (q/\varepsilon)[-N_D d^2/2 + (N_A W + n_s)(d + a)] \qquad (1)$$

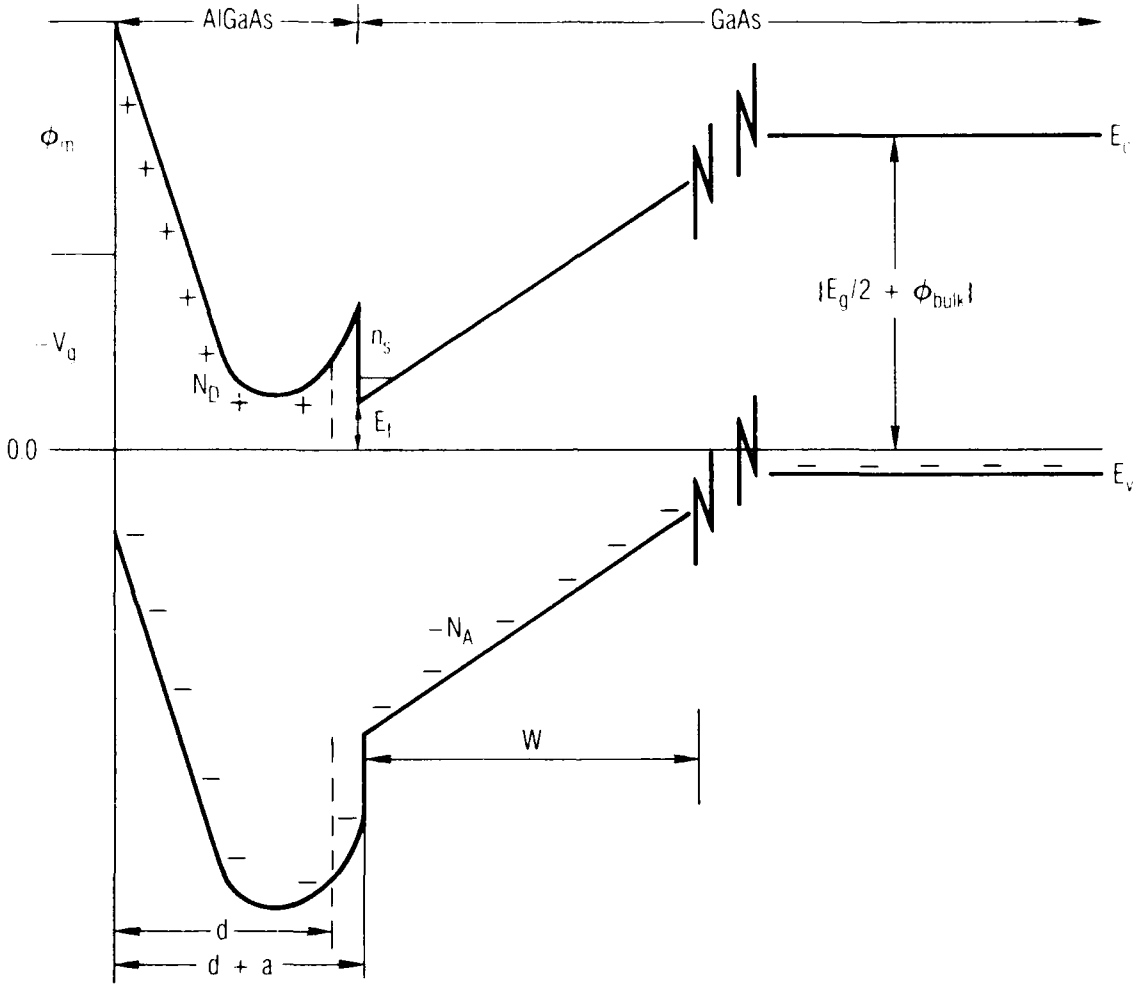

Fig. 1. Band Diagram of a Typical AlGaAs/GaAs MODFET with Schottky Gate, under Bias V_g

where

ΔE_c = conduction band offset

In the one-subband approximation, the Fermi level E_f may be calculated as

$$E_f = E_0/q + (kT/q)\ln[\exp(\pi\hbar^2 n_s/m_1 kT) - 1] \quad (2)$$

where the first quantum level E_0 may be calculated in the triangular-well approximation and is given by

$$E_0 = (9\hbar^2/8m_1)(4E_i m_1/\hbar^2)^{2/3} \quad (3)$$

The field E_i at the interface is

$$E_i = (q/\epsilon)(n_s + N_A) \quad (4)$$

Substitution of Eqs. (2-4) into Eq. (1) yields

$$V_g = V_0 + f(n_s) \quad (5)$$

where

$$V_0 = \Phi_m - \Delta E_c - (q/\epsilon)N_D d^2/2 \quad (6)$$

The function $f(n_s)$ may be written as

$$f(n_s) = (q/\epsilon)(d + a)(N_A W + n_s) + C_0(N_A W + n_s)^{2/3}$$

$$+ (kT/q)\ln[\exp(n_s/n_c) - 1] \quad (7)$$

where

$$C_0 = (9\hbar^2/8m_1 q)(4q^2 m_1/\hbar^2\varepsilon)^{2/3} \qquad (8)$$

$$= [\sim 1.7 \times 10^{-9}\ \text{V-cm}^{4/3}]$$

$\hbar$ = Planck constant divided by 2π

m_1 = longitudinal effective mass of the carriers

We have retained terms containing the depletion width W in the definition of $f(n_s)$ because the depletion width is implicitly a function of the channel charge n_s.

The quantities q, ε, k, and T are the elemental charge, AlGaAs(GaAs) permittivity (assumed identical), Boltzmann constant, and absolute temperature.

Similarily, charge density n_c is a function of physical constants and the effective carrier mass:

$$n_c = \pi\hbar^2/m_1 kT \qquad (9)$$

and is equal to $\sim 8.4 \times 10^{11}\ \text{cm}^{-2}$.

A discussion of the dependence of the depletion width W on acceptor density has been given elsewhere (Ref. 1). In section II we describe the mathematical properties of the function $f(n_s)$, in the high channel carrier density region, and exploit the results to describe the characteristics of these devices.

II. HIGH DENSITY REGION

A. DEFINITION

We define the high density region such that $n_s > n_c$ over the whole channel. In this region Eq. (7) may be expanded in a Taylor series in n_s about n_c. The results of this approximation to first order are shown in Fig. 2 for two extremes of acceptor doping density. The solid lines are the results of Eq. (7), and the dashed lines are the result of the first order expansion in n_s about n_c. Above n_c (8.4×10^{11} cm^{-2}), the expansion is quite good. Much below n_c ($< 3.0 \times 10^{11}$ cm^{-2}), the first order expansion departs from the exact result and approaches a constant. Substitution of the first order expansion for $f(n_s)$ in Eq. (5) and inverting to find n_s as a function of V_g yields

$$n_s = n_c + K^{-1}[V_g - V_0 - f(n_c)]/(kT/q) \qquad (10)$$

where K is a constant that depends on the device geometry, doping densities, depletion width, and physical constants. This form for n_s is different than previously assumed (Ref. 5), which ignores the contribution from n_c and from $f(n_c)$ and assumes that the reciprocal of K is the AlGaAs layer capacitance per unit area per unit charge times the absolute temperature in electron volts. In our formulation, near saturation, K is given by:

$$K = (q/kT)(q/\varepsilon)(d + a) + (2/3)C_0(q/kT)/(N_A W + n_c)^{1/3} + 1.58/n_c \qquad (11)$$

B. DEVICE CAPACITANCE

The derivative of Eq. (10) with respect to V_g yields the device capacitance per unit area, which may be written in the following form (Ref. 6):

$$C_{area} = \varepsilon/(d + a + \Delta d) \qquad (12)$$

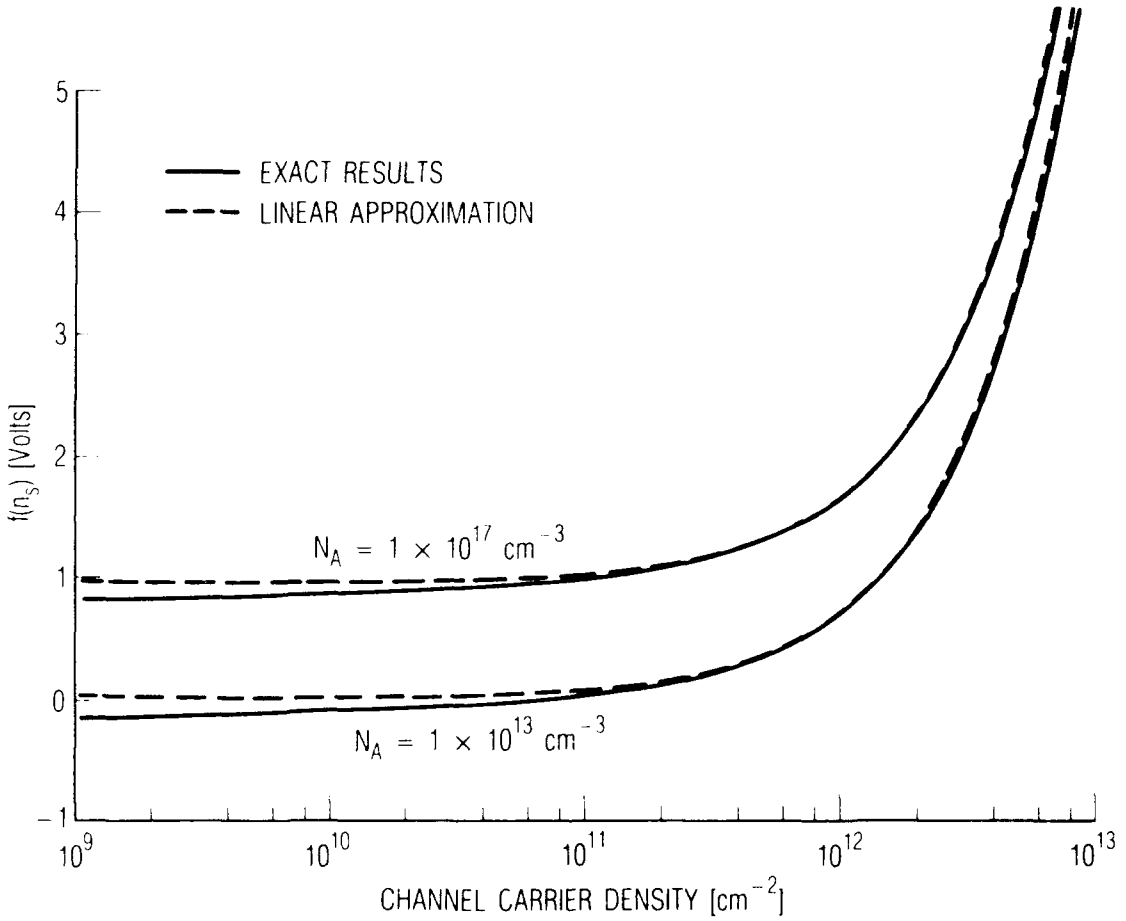

Fig. 2. Function $f(n_s)$ versus Channel Carrier Density for Two Extremes of Acceptor Density. The solid curves are the exact results of Eq. (2); the dashed lines are the results of the linear approximation, described in text.

where Δd is invoked to account for the discrepancy between the AlGaAs layer capacitance $\varepsilon/(d + a)$ and the device capacitance. Taking the derivative of Eq. (10) and using Eq. (12) to solve for Δd yields

$$\Delta d = (2.3q)C_0^{-1}(N_A W + n_c)^{1/3} + 1.58(kT/q)(\varepsilon/q)^{-1} n_c \qquad (13)$$

For low acceptor densities ($< 10^{13}$ cm^{-3}), Δd levels off at a value of ~89 Å, which is in good agreement with values cited in the literature (Ref. 5). As the acceptor density increases, Δd decreases. At an acceptor density of 10^{17} cm^{-3}, Δd decreases to ~74 Å.

C. EXPERIMENTAL THRESHOLD VOLTAGE

MODFET threshold voltages are determined experimentally by extrapolating the saturation current, or square root of the saturation current, versus gate voltage to zero. The gate voltage intercept is the experimentally determined threshold voltage. We may approximate the experimental threshold voltage by solving Eq. (10) for the gate voltage when n_s is equal to zero. This yields a threshold voltage which differs from the strong inversion definition of threshold voltage (Ref. 1). The difference between this approximation for the threshold voltage and the strong inversion threshold voltage is given by

$$V_{th} = f(n_c) - f(n_{th}) - qn_c C_{area} \qquad (14)$$

where the channel charge at threshold n_{th} is equal to the acceptor density N_A, times the average channel width z_{av}, which may be calculated in the triangular-well approximation using variational functions (Refs. 7, 8). This definition of threshold has been described elsewhere (Ref. 1).

In Fig. 3 the threshold voltage difference, Eq. (14), is plotted versus acceptor density. Each term in Eq. (14) is plotted separately. At low acceptor densities ($< 10^{14}$ cm^{-3}) the difference may be as much as 0.25 V. This difference decreases as the acceptor density increases. As this difference depends on the acceptor density, a comparison of

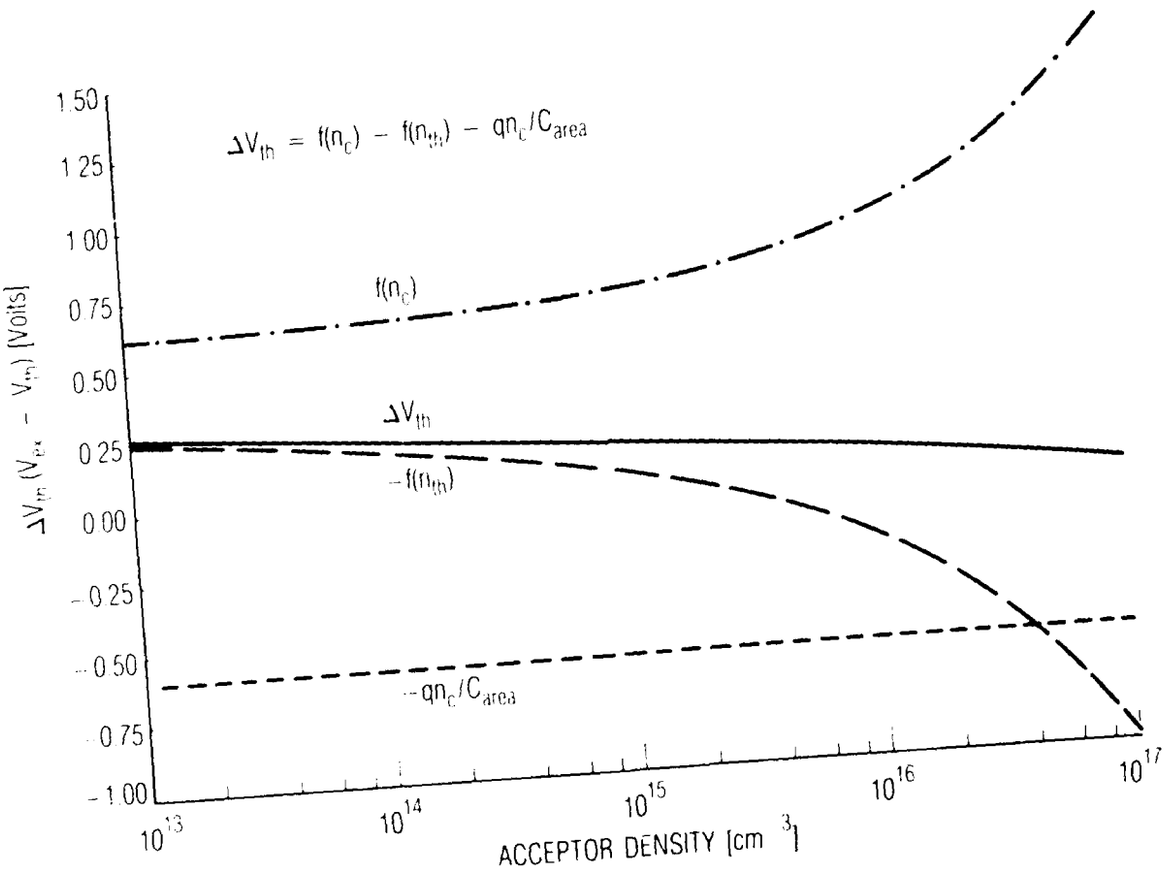

Fig. 3. Difference between Experimental and Theoretical Threshold Voltage versus Acceptor Density

experimental threshold voltages may not be appropriate if acceptor densities differ by a significant amount.

D. I-V CHARACTERISTICS

In the gradual channel approximation, charge control is determined by the effective potential in the channel:

$$V(x) = V_g - V_c(x) \tag{15}$$

where $V_c(x)$ is the channel voltage under the gate at point x. Using Eq. (10) we solve for the carrier density in the channel:

$$n_s(x) = n_c + K^{-1}[V_g - V_0 - f(n_c) - V_c(x)]/(kT/q) \tag{16}$$

The form of Eq. (16) allows the source-drain current to be calculated in the usual way (Ref. 5). The result is

$$I_{HD} = q(Z/L)u\{n_c + [(C_{area}/q)(V_g-V_0-f(n_c))][V_c(L)-V_c(0)] - (C_{area}/q)[V_c^2(L)-V_c^2(0)]\} \tag{17}$$

where u is the channel mobility and Z/L is the gate-width to gate-length ratio. For a grounded source, in the limit of zero source-drain resistance, we recover the usual dependence on drain voltage.

In the development of Eq. (17) we have assumed that each point in the channel has a carrier density greater than n_c. This places a limit on the bias conditions for the applicability of Eq. (17). Evaluating Eq. (16) at the drain contact and using the condition that $n_s(L)$ must be greater than n_c, yields the following limitations on the bias conditions for a grounded source and zero source-drain resistance:

$$(V_g-V_D) > V_0 + f(n_c) \tag{18}$$

where V_D is the drain voltage. Shown in Fig. 4(a) is I_{DS} versus V_D for a grounded source and zero source-drain resistance for various acceptor doping densities and the device parameters shown. The heavy dots indicate the point at which the calculation is no longer valid by virtue of Eq. (18). As the acceptor density increases, the current at a given drain voltage decreases and the limit of the applicability of the calculation decreases, in drain voltage, for a given gate voltage. A similar graph is shown in Fig. 4(b) in which I_{DS} versus V_D is shown for a given acceptor density and various gate voltages. As the gate voltage decreases, the current at a given drain voltage decreases, as expected, and the region of applicability of the calculation, in drain voltage, decreases. This result implies that using an equation of the form given in Eq. (17), which results from a linearization of $f(n_s)$ above n_e, to infer the nature of the saturation characteristics in MOSFETs, in which the drain portion of the channel has a channel carrier density much less than n_e, is suspect (Ref. 5).

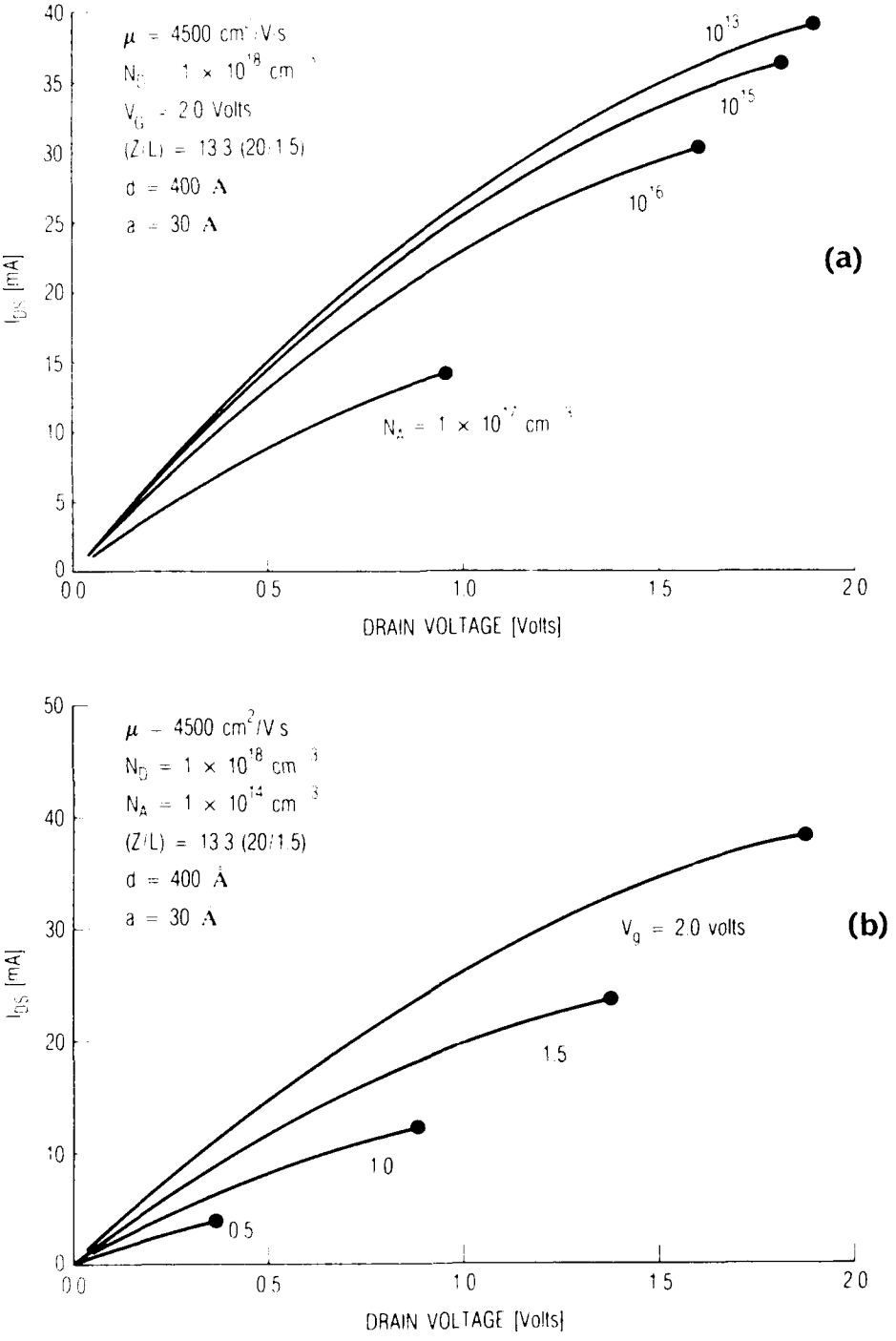

Fig. 4. Drain-Source Current versus Drain Voltage for Various Acceptor Densities (a), and Various Gate Voltages (b). Heavy dots indicate the limits of the calculation as given by Eq. (11) in the text.

III. SUMMARY

We have developed a triangular-well, one-subband depletion layer model to describe the high channel density operation of MODFETs. The effects of acceptor density on the I-V characteristics in the high channel density region has been investigated. The depletion layer charge, due to ionized acceptors, is shown to account for the discrepancy between the device capacitance and the AlGaAs layer capacitance, as described in the literature (Ref. 6). The depletion layer charge also accounts for the discrepancy between the theoretical threshold voltage, in the strong inversion model (Ref. 1), and the experimental threshold voltage, as determined by extrapolation of the source-drain current. Therefore, comparison of threshold voltage characteristics, particularly for devices with appreciably different acceptor densities, should be based on a consistent description of threshold that accounts for ionized acceptors, i.e., the strong inversion model.

REFERENCES

1. R. J. Krantz and W. L. Bloss, "The Role of Unintentional Acceptor Concentration on the Threshold Voltage of Modulation-Doped Field-Effect Transistors," IEEE Trans. Electron Devices ED-36, 451-53 (February 1989).

2. R. J. Krantz, W. L. Bloss, and M. J. O'Loughlin, "High Energy Neutron Effects in GaAs Modulation-Doped Field Effect Transistors (MODFETs): Threshold Voltage," IEEE Trans. Nuc. Sci. NS-35, 1438-43 (December 1988).

3. R. J. Krantz and W. L. Bloss, "Threshold Voltage and I-V Characteristics of AlGaAs/GaAs MODFETs," accepted for publication in The Proceedings of the 1989 Industry-University Advanced Materials Conference, Denver, Colorado, March 6-9, 1989.

4. R. J. Krantz and W. L. Bloss, "Subthreshold I-V Characteristics of AlGaAs/GaAs MODFETs: The Role of Unintentional Acceptors," accepted for publication in IEEE Trans. Electron Devices.

5. D. Delagebeaudeuf and N. T. Linh, "Metal-(n) AlGaAs-GaAs Two-Dimensional Electron GaAs FET," IEEE Trans. Electron Devices, ED-29, 955-60 (June 1982).

6. K. Lee, M.S. Shur, T.J. Drummond, and H. Morkoc, "Current-Voltage and Capacitance-Voltage Characteristics of Modulation-Doped Field-Effect Transistors," IEEE Trans. Electron Devices ED-30, 207-12 (1983).

7. F. F. Fang and W. E. Howard, "Negative Field-Effect Mobility on (100) Si Surfaces," Phys. Rev. Lett. 16, 797-99 (1966).

8. F. Stern and W. E. Howard, "Properties of Semiconducting Surface Inversion Layers in the Electric Quantum Limit," Phys. Rev. 163, 816-35 (1967).

LABORATORY OPERATIONS

The Aerospace Corporation functions as an "architect-engineer" for national security projects, specializing in advanced military space systems. Providing research support, the corporation's Laboratory Operations conducts experimental and theoretical investigations that focus on the application of scientific and technical advances to such systems. Vital to the success of these investigations is the technical staff's wide-ranging expertise and its ability to stay current with new developments. This expertise is enhanced by a research program aimed at dealing with the many problems associated with rapidly evolving space systems. Contributing their capabilities to the research effort are these individual laboratories:

Aerophysics Laboratory: Launch vehicle and reentry fluid mechanics, heat transfer and flight dynamics; chemical and electric propulsion, propellant chemistry, chemical dynamics, environmental chemistry, trace detection; spacecraft structural mechanics, contamination, thermal and structural control; high temperature thermomechanics, gas kinetics and radiation; cw and pulsed chemical and excimer laser development, including chemical kinetics, spectroscopy, optical resonators, beam control, atmospheric propagation, laser effects and countermeasures.

Chemistry and Physics Laboratory: Atmospheric chemical reactions, atmospheric optics, light scattering, state-specific chemical reactions and radiative signatures of missile plumes, sensor out-of-field-of-view rejection, applied laser spectroscopy, laser chemistry, laser optoelectronics, solar cell physics, battery electrochemistry, space vacuum and radiation effects on materials, lubrication and surface phenomena, thermionic emission, photosensitive materials and detectors, atomic frequency standards, and environmental chemistry.

Electronics Research Laboratory: Microelectronics, solid-state device physics, compound semiconductors, radiation hardening; electro-optics, quantum electronics, solid-state lasers, optical propagation and communications; microwave semiconductor devices, microwave/millimeter wave measurements, diagnostics and radiometry, microwave/millimeter wave thermionic devices; atomic time and frequency standards; antennas, rf systems, electromagnetic propagation phenomena, space communication systems.

Materials Sciences Laboratory: Development of new materials: metals, alloys, ceramics, polymers and their composites, and new forms of carbon; nondestructive evaluation, component failure analysis and reliability; fracture mechanics and stress corrosion; analysis and evaluation of materials at cryogenic and elevated temperatures as well as in space and enemy-induced environments.

Space Sciences Laboratory: Magnetospheric, auroral and cosmic ray physics, wave-particle interactions, magnetospheric plasma waves; atmospheric and ionospheric physics, density and composition of the upper atmosphere, remote sensing using atmospheric radiation; solar physics, infrared astronomy, infrared signature analysis; effects of solar activity, magnetic storms and nuclear explosions on the earth's atmosphere, ionosphere and magnetosphere; effects of electromagnetic and particulate radiations on space systems; space instrumentation.